

Strongly Coupled Ruthenium–Polypyridyl Complexes for Efficient Electron Injection in Dye-Sensitized Semiconductor Nanoparticles

G. Ramakrishna,[†] D. Amilan Jose,[‡] D. Krishna Kumar,[‡] Amitava Das,^{*,‡} Dipak K. Palit,[†] and Hirendra N. Ghosh^{*,†}

Radiation Chemistry & Chemical Dynamics Division, Bhabha Atomic Research Center, Trombay, Mumbai 400 085, India, and Central Salt and Marine Chemicals Research Institute, Bhavnagar 364002, Gujarat, India

Received: March 12, 2005; In Final Form: May 28, 2005

Dynamics of interfacial electron transfer (ET) in the ruthenium–polypyridyl complex [$\{\text{bis}(2,2'\text{-bpy})\text{-(4-[2-(4'-methyl-2,2'-bipyridinyl-4-yl)vinyl]benzene-1,2-diol)}\}$ ruthenium(II) hexafluorophosphate] (Ru-cat)-sensitized TiO_2 nanoparticles has been investigated using femtosecond transient absorption spectroscopy detecting in the visible and near-infrared region. It has been observed that Ru-cat is coupled strongly with the TiO_2 nanoparticles through its pendant catechol moiety. Electron injection has been confirmed by direct detection of electrons in the conduction band, cation radical of the adsorbed dye, and a bleach of the dye in real time as monitored by transient absorption spectroscopy. A single-exponential and pulse width limited (<100 fs) electron injection has been observed, and the origin of it might have been from the nonthermalized excited states of the Ru-cat molecule. The result gave a strong indication that the electron injection competes with the thermalization of the photoexcited states due to large coupling elements for the forward ET reaction. Back-ET dynamics has been determined by monitoring the decay kinetics of the cation radical and injected electron and also from recovery kinetics of the bleach of the adsorbed dye. It has been fit with a multiexponential function, where $\sim 30\%$ of the injected electrons are recombined with a time constant of <2 ps, again indicating large coupling elements for the charge recombination reaction. However, our results have shown relatively long-lived charge separation in the Ru-cat/ TiO_2 system as compared to other organic dye-sensitized TiO_2 nanoparticles with similar interactions.

1. Introduction

Relentless efforts are underway all over the world in understanding the dye sensitization of wide band gap semiconductor nanomaterials (e.g., TiO_2 , SnO_2 , ZnO) in view of their potential technological implication in photovoltaic energy.^{1,2} In this area maximum effort has been focused on dye molecules based on metal–polypyridine complexes and their analogues.^{2–5} So far, tris(bipyridyl)ruthenium(II) dyes have been regarded as the best sensitizing dyes for solar energy conversion for their strong visible absorption bands, long-lived excited states, and excellent photochemical stability. One has to optimize several characteristics of these polypyridine complex molecules such as high electron injection efficiency from the metal-to-ligand charge transfer (MLCT) excited state to the conduction band of the semiconductor, slow back electron transfer (BET), broad absorption in the entire visible and NIR region, and also high affinity for the TiO_2 surface, which is provided by the anchoring groups of the sensitizer molecules. In most of the studies the anchoring groups of the dye molecules used in dye-sensitized solar cell including those polypyridine complexes are carboxylate, which bind the dye molecules with the nanoparticles. However, there are certain disadvantages to use carboxylates as anchoring groups. The ground-state $\text{p}K_a$ of the carboxylates is too low to ensure strong binding.⁶ Also, slow desorption of

the photosensitizers can occur in the presence of water which may limit the long-term stability of the cell.

Recent studies have revealed that organic or inorganic molecules containing pendant catechol moiety can be very good sensitizers for TiO_2 nanoparticles. Catecholate type of binding not only facilitates efficient electron injection but also anchors the dye strongly to the semiconductor surface even at higher pH conditions. There is only one report available in the literature by Rice et al.⁷ where catechol type of binding is used for anchoring the Ru(II)–polypyridyl complexes onto the TiO_2 semiconductor nanoparticles. It has been reported that the grafting properties of the complexes containing catechol functional groups with the TiO_2 surface are superior as compared to the complexes containing carboxylic acid group. In principle, Ru(II)–polypyridyl complexes with pendant catechol moiety used by Rice et al.⁷ are expected to show very high photon to current conversion ratio. Despite very effective anchoring of those complex molecules on the TiO_2 surface, the measured IPCE values are lower than those obtained for related complexes using a carboxylate anchoring group. The real reason behind the lower efficiency in IPCE is still unclear.

Dynamics of interfacial ET in the Ru(II)–polypyridyl complex-sensitized TiO_2 nanocrystalline material has created an immense debate as many researchers reported a variety of electron injection rates.^{8–13} Most of the workers have reported the presence of ultrafast component (sub-100 fs) in the dynamics of electron injection. According to Lian and co-workers,^{9,10} the ultrafast component is the major constituent in the electron injection process. On the other hand, many groups^{10–13} have

[†] Bhabha Atomic Research Center.

[‡] Central Salt and Marine Chemicals Research Institute.

* Corresponding author: e-mail hngosh@magnum.barc.ernet.in; Fax 00-91-22-25505151.

reported additional components of slower electron injection with a distribution of time constants of 1 ps to tens of picoseconds. In some cases, reasons behind nonexponential electron injection time constants were given as the heterogeneity of the semiconductor/dye systems.¹⁴ More importantly, in addition to electron injection, the photoexcited Ru(II)–polypyridyl dye molecules are known to undergo a number of ultrafast relaxation processes.¹⁵ These processes are expected to be in parallel or competing with electron injection process. This might be the reason for electron injection from both nonthermalized and thermalized states of the photoexcited Ru(II)–polypyridyl dye molecule. As a result, many researchers^{9–13} have witnessed a multiexponential electron injection process for Ru(II)–polypyridyl complex-sensitized TiO₂ nanocrystalline system. At this juncture, it is important to know whether it is possible to inject electrons from the nonthermalized state, circumventing the other ultrafast relaxation processes in photoexcited Ru(II)–polypyridyl complexes. As we have mentioned earlier that most of the sensitizing Ru–polypyridyl complexes which have shown multiexponential electron injection kinetics are bound with TiO₂ nanomaterial through a carboxylic group. Binding of the carboxylic acid group with the semiconductor is relatively weak, which allows the photoexcited Ru–polypyridyl complexes to relax to thermalized states and eventually inject electron from those states. As a result, one can expect multiexponential electron injection time constants.

Polypyridyl complexes with a pendant catechol moiety can show considerable promise in the context of realizing the phenomenon of the electron injection from nonthermalized states of the dye molecule. It has been suggested theoretically by Rego et al.¹⁶ that, contrary to the direct charge-transfer excitation in TiO₂–catechol (and its derivatives¹⁷) systems, efficient photo-injection mechanisms can involve electronic excited states in the molecular adsorbate in the Ru(II)–polypyridyl–catecholate. The ultrafast study of electron injection investigated in this work is aimed at gaining a fundamental understanding of such excited-state electron injection paths. To see electron injection from the nonthermalized state, it is very important to have strong coupling between the sensitizer molecule and semiconductor nanoparticles. Catechol binding with TiO₂ nanoparticles through a five-membered chelate formation is expected to be thermodynamically very stable. In our previous studies we have shown that pyrogallol red (PGR),¹⁸ bromopyrogallol red (Br-PGR),¹⁸ and alizarin¹⁹ molecules bind strongly with TiO₂ nanoparticles through the catechol moiety and found to have large electronic coupling with the TiO₂. Electron injection was found to be single-exponential and pulse width limited in all those systems.^{18,19} Thus, to have a strongly coupled Ru(II)–polypyridyl center with nanoparticulate TiO₂, we have used Ru-cat, which consists of a pendant catechol moiety. In the present investigation, we have carried out femtosecond transient absorption measurements in Ru-cat-sensitized TiO₂ nanoparticles to study interfacial ET dynamics and also to understand the influence of electronic coupling on interfacial ET dynamics.

2. Materials and Method

Sample Preparation: (a) **Materials.** Titanium(IV) tetraisopropoxide {Ti[OCH(CH₃)₂]₄} (Aldrich, 97%) and isopropyl alcohol (Aldrich) were purified by distillation. Nanopure water (Barnsted System) was used for making aqueous solutions.

(b) **Synthesis of {Bis(2,2′-bpy)-(4-[2-(4′-methyl-2,2′-bipyridinyl-4-yl)vinyl]benzene-1,2-diol)} Ruthenium(II) Hexafluorophosphate (Ru-cat).** This was synthesized by adopting the reported procedure²⁰ with some modification in the purification

procedure. Ru(2,2-bipy)₂Cl₂·2H₂O (0.156 g, 0.30 mmol) and 4-[2-(4′-methyl-2,2′-bipyridinyl-4-yl)vinyl]benzene-1,2-diol (0.110 g, 0.36 mmol) were reacted in 25 mL of ethanol for 6 h, and then the volume was reduced in vacuo to ~5 mL. To this saturated aqueous solution, KPF₆ was added and kept refrigerated for 2 h. The red precipitate thus obtained was filtered off, washed with cold water, and air-dried. This crude product was first purified by gravity chromatography using silica as stationary phase and CH₃CN(aq)–NH₄PF₆ (98/2, v/v) as eluent. The main orange fraction was collected and dried in vacuo. Excess NH₄PF₆ was removed in the aqueous layer by solvent extraction from CH₂Cl₂ solution. This CH₂Cl₂ solution was again dried and was further purified by chromatography using neutral alumina (Grade III) column and CH₃CN–C₆H₅CH₃ (7/3, v/v) as eluent. The first major fraction was collected and dried in vacuo to yield the desired compound in pure form. Yield: 0.19 g; 63%. Elemental analysis and spectroscopic (FTIR, ¹H NMR, UV–vis and luminescence) data are similar to that reported earlier.

(c) **Sample Preparation.** Nanometer-size TiO₂ was prepared by controlled hydrolysis of titanium (IV) tetraisopropoxide.^{21–23} A solution of 5 mL of Ti[OCH(CH₃)₂]₄ (Aldrich, 97%) dissolved with 95 mL of isopropyl alcohol (Aldrich) was added dropwise (1 mL/min) to 900 mL of Nanopure water (2 °C) at pH 1.5 (adjusted with HNO₃). The solution was continuously stirred for 10–12 h until a transparent colloid was formed. The colloidal solution was concentrated at 35–40 °C with a rotary evaporator and then dried with nitrogen stream to yield a white powder. In the present work all colloidal samples were prepared after dispersing the dry TiO₂ nanoparticles in water (15 g/L). A transparent clear solution of TiO₂ nanoparticle was formed. We have carried out sensitization of nanoparticles by adding solid Ru-cat in to the aqueous colloids under continuous stirring conditions. As Ru-cat is not soluble in water, the solvation process supports the coupling Ru-cat with both the semiconductor nanoparticles (TiO₂ and ZrO₂). Through other procedures we have sensitized the nanoparticles, by presolving Ru-cat in methanol and then the adding dissolved dye into the aqueous colloidal solution (net volume fraction < 5% methanol). The resulting solution is kept for half an hour in stirring conditions for the dye to covalently bind to nanoparticulate TiO₂. For all the measurements the sample solutions were deoxygenated by continuously bubbling high-purity nitrogen (99.95 IOLAR grade from Indian Oxygen Co. Ltd., India) through the solutions. The solutions were passed through a 2 mm path length quartz cell during all the measurements.

(d) **Femtosecond Visible Spectrometer:** The femtosecond tunable visible spectrometer has been developed based on a multipass amplified femtosecond Ti:sapphire laser system from Avesta, Russia (1 kHz repetition rate at 800 nm, 50 fs, 800 μJ/pulse) and described earlier.^{24,25} The 800 nm output pulse from the multipass amplifier is split into two parts to generate pump and probe pulses. In the present investigation we have used both 800 nm (fundamental) and its frequency-doubled 400 nm as excitation sources. To generate pump pulses at 400 nm, one part of 800 nm with 200 μJ/pulse is frequency-doubled in BBO crystals. To generate visible probe pulses, about 3 μJ of the 800 nm beam is focused onto a 1.5 mm thick sapphire window. The intensity of the 800 nm beam is adjusted by iris size and ND filters to obtain a stable white light continuum in the 400 nm to over 1000 nm region. The probe pulses are split into the signal and reference beams and are detected by two matched photodiodes with variable gain. We have kept the spot sizes of the pump beam and probe beam at the crossing point

around 500 and 300 μm , respectively. The excitation energy density (at both 800 and 400 nm) was adjusted to $\sim 2500 \mu\text{J}/\text{cm}^2$. The noise level of the white light is about $\sim 0.5\%$ with occasional spikes due to oscillator fluctuation. We have noticed that most laser noise is low-frequency noise and can be eliminated by comparing the adjacent probe laser pulses (pump blocked vs unblocked using a mechanical chopper). The typical noise in the measured absorbance change is about $<0.3\%$. The instrument response function was obtained by fitting the rise time of the bleach of sodium salt of *meso*-tetrakis(4-sulfonatophenyl)porphyrin (TPPS) at 710 nm, which has an instantaneous response.

(e) Microsecond Flash Photolysis. The microsecond laser flash photolysis experiment was carried out using a picosecond laser spectrometer described in details elsewhere.²⁶ The second harmonic output pulse (532 nm, 35 ps, 15 mJ) from an active-passively mode-locked Nd:YAG laser was used as a pump pulse. A tungsten lamp was used as the analyzing light. A Bausch & Lomb monochromator, a PMT (Hamamatsu R-928), and a digital oscilloscope (Tektronics TDS-540, 500 MHz bandwidth) which is connected to a computer were used for detection and recording of the kinetic traces.

(f) Pulse Radiolysis. Transient absorption studies were carried out using the pulse radiolysis technique described earlier.²⁷ Electron pulses of 7 MeV and 50 ns duration were used for irradiation. The transients produced were detected by a kinetic spectrophotometer. The absorbed radiation dose was measured by thiocyanate dosimetry, and the typical dose was 10 Gy.

(g) Cyclic Voltammetry. Electrochemical experiments with Ru-cat in solution were performed on a CH-660A electrochemical instrument; a conventional three-electrode cell assembly was used. A saturated Ag/AgCl electrode was used as reference, and platinum was used as working electrode for all measurements. Ferrocene was added at the end of each experiment as internal standard, and all potentials are quoted vs the ferrocene/ferrocenium (Fc/Fc^+) couple. The oxidation redox potential of the Ru-cat molecule has been determined to be 1.32 V against Ag/AgCl electrode.

3. Results and Discussion

(a) Dye Binding with TiO_2 Nanoparticles. The nature of the binding between a sensitizer and a semiconductor directly influences the excited-state and interfacial ET behavior.²⁸ A strong binding serves to anchor the sensitizer in place, control interfacial electronic coupling, and tune the redox potentials of the sensitizers and the semiconductor. Effects of surface anchoring groups (carboxylate vs phosphonate) in ruthenium-complex-sensitized TiO_2 nanoparticles on visible light reactivity in aqueous suspensions have been clearly demonstrated by Bae et al.²⁹ The pH-dependent reactivity of their systems has indicated that the chemical bond formation between the phosphonic acid ($-\text{PO}_3\text{H}_2$) and the TiO_2 hydroxyl group ($\equiv\text{Ti}-\text{OH}$) is highly favored over the ester linkage ($\equiv\text{Ti}-\text{OCO}-\text{R}$) formation. In this respect, the phosphonic acid group is more suitable as a stable linkage to TiO_2 surface. However, the affinity of catechol dye molecules toward TiO_2 semiconductor nanoparticles is better as compared to the carboxylate or phosphate dye molecules, which can establish a better linkage over the other two. To understand the mechanism of the Ru-cat-sensitized ET reaction in the dye–nanoparticles system, it is very important to know the type of interaction between the Ru-cat and the nanoparticles when they get adsorbed on the nanoparticle surface. Optical absorption spectra of $\text{Ru}(\text{II})$ –polypyridyl complexes with carboxylate as anchoring group

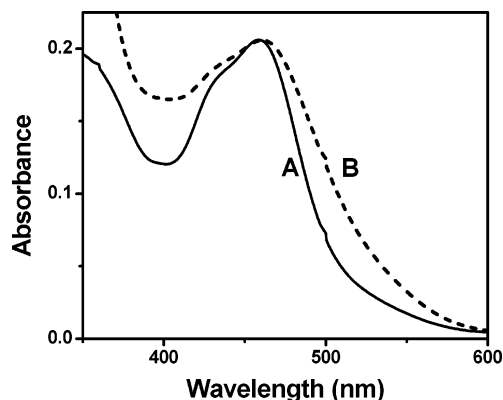


Figure 1. Normalized optical absorption spectrum of Ru-cat in water (A) and on TiO_2 nanoparticle (10 g/L) surface (B). pH for both the systems were kept ~ 2.5 .

changes marginally in the presence of TiO_2 nanoparticles.^{30,31} On the other hand, it has been observed by us^{18,19} and many others^{17,32} that sensitizer molecules which possess a catechol moiety as anchoring group has very strong electronic interaction with TiO_2 nanoparticles. To understand the same, optical absorption measurements of Ru-cat in water and in the presence of TiO_2 colloidal solutions have been carried out. Figure 1 shows the optical absorption spectrum of free Ru-cat in water and Ru-cat adsorbed on TiO_2 nanoparticles at pH 2.5. Ru-cat in water shows an absorption peak at 458 nm (Figure 1). This low-energy band can be attributed to two overlapping $d_{\text{Ru}(\text{II})} \rightarrow \pi^*_{(\text{bpy})}$ (MLCT)-based transitions—one due to $d_{\text{Ru}(\text{II})} \rightarrow \pi^*_{(2,2'-\text{bpy})}$ -based (at ~ 452 nm) and the other one is due to $d_{\text{Ru}(\text{II})} \rightarrow \pi^*_{(\text{bpy}-\text{cat})}$ -based (at ~ 458 nm). Since the excitation wavelength is 400 nm in the transient absorption measurements, we have not spent much attention to characterize the higher energy bands of Ru-cat complexes. However, there is an indication of the bpy-cat ligand based $\pi-\pi^*$ transitions, which can have its tail at 400 nm. Upon addition of TiO_2 nanoparticles, absorption spectrum of Ru-cat becomes broad and shifted to longer wavelength with an appreciable increase in absorbance of the band at 465 nm. The red shift and broadening of the visible band at 465 nm of Ru-cat in the presence of TiO_2 can be attributed to the strong interaction between the sensitizer and nanoparticles. In our previous work, we have discussed that the interaction between TiO_2 nanoparticles and dye molecules like alizarin¹⁹ and triphenylmethane (TPM) dyes¹⁸ (pyrogallol red and bromopyrogallol red) is very strong. Cherepy et al.³² have also reported the strong interaction between anthocyanine dye and TiO_2 nanoparticles. Interestingly, all the above dyes (alizarin, TPM, and anthocyanine) has a catechol moiety, which can interact strongly with TiO_2 nanoparticles. TiO_2 nanoparticles can form a strong complex through a catechol moiety of the dye molecules with formation of a five-membered ring (Chart 1). It has already been discussed by Moser et al.³³ that TiO_2 nanoparticles form strong complex with catechols with the formation of a five-membered ring. Rajh et al.³⁴ have also reported similar formation of CT complex of TiO_2 nanoparticles for a series of enediol compounds. From the optical absorption studies, it can be conclusively emphasized that Ru-cat interacts strongly with TiO_2 nanoparticles with the formation of a five-membered complex, as shown in the Chart 1.

(b) Excited-State Dynamics of Free Ru-cat in Acetonitrile and on Nonreactive Surface. To comprehend the detailed ET dynamics in Ru-cat-sensitized TiO_2 nanoparticles, understanding of the excited-state dynamics of the sensitizer molecules themselves without the complication of electron injection is

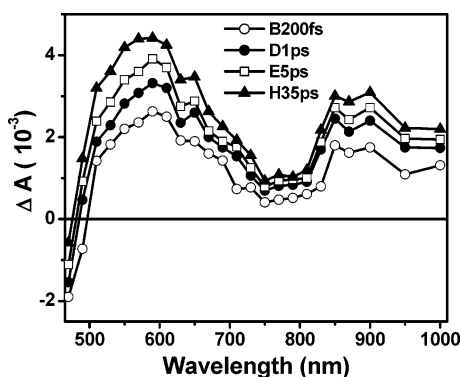
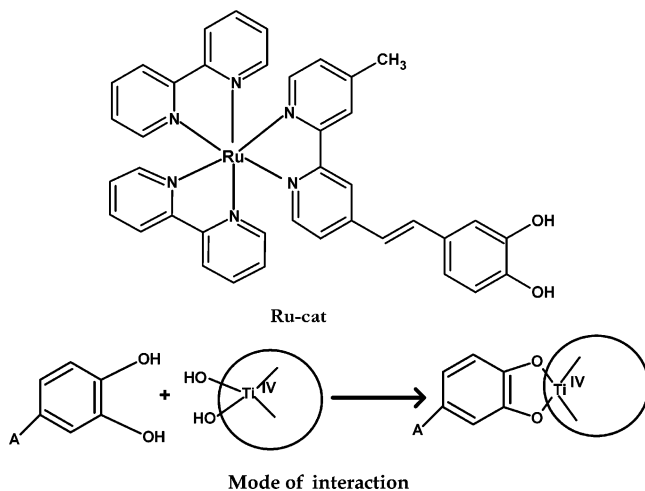


Figure 2. Transient absorption spectra of Ru-cat in acetonitrile at different delay times. The transient absorption spectrum has maxima at 590 and 900 nm, which have been attributed to the $^3\text{MLCT}$ band (triplet–triplet absorption).

CHART 1: Molecular Structure of Ru-cat, and Schematic Illustration of the Complexation Reaction between the Hydroxylated TiO_2 Surface and Ru-cat through Catechol Type Binding



necessary. For the same reason, excited-state dynamics of Ru-cat in acetonitrile and Ru-cat adsorbed on ZrO_2 nanoparticles (a large band gap substrate) has been investigated. Shown in Figure 2 are the transient absorption spectra at different time delays of Ru-cat in acetonitrile after excitation at 400 nm. The transients show two major absorption peaks, in the wavelength region 480–750 nm centered around 590 nm and another in 830–950 nm region with a maximum at 900 nm. The transient absorption bands can be ascribed to the excited-state absorption (ESA) of Ru-cat. It has been reported in recent literature³⁵ that the intersystem crossing (ISC) process (singlet to triplet) is very fast (<50 fs) for the Ru–polypyridyl complexes. Consequently, in the present investigation, we have attributed the ESA to the excited triplet state absorption, as it is believed that the singlet to triplet conversion might have occurred within the pulse width of the instrument. It is interesting to observe that the amplitude of the transient absorption increases with time (Figure 2), and after a certain time delay it does not decay up to 400 ps. Figure 3 shows transient absorption kinetics at 900 nm for Ru-cat in acetonitrile (Figure 3A) and in ZrO_2 colloids (Figure 3B). It has been observed in the figure that both the kinetic traces have two growth time constants. The kinetic trace in Figure 3A has been best fitted with time constants of <100 fs (72%) and 19 ps (28%), and Figure 3B has been best fit with time constants of <100 fs (81.4%) and 10 ps (18.6%). First growth component in both are pulse width limited (<100 fs), which can be

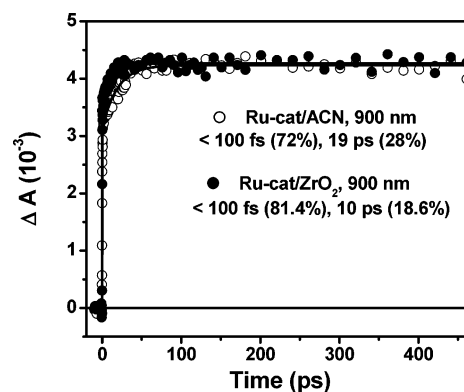
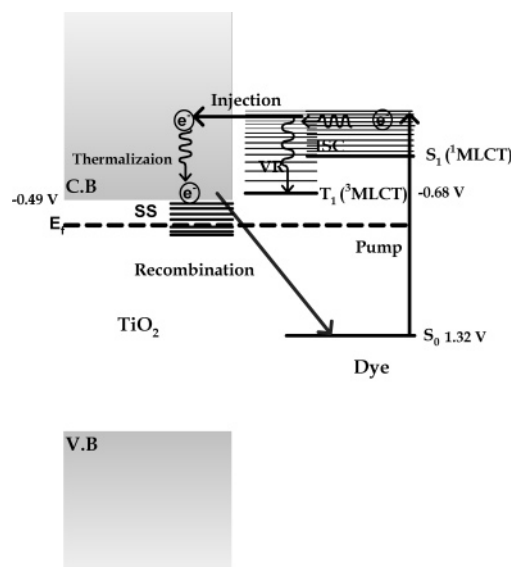


Figure 3. Kinetic trace of the triplet state ($^3\text{MLCT}$) of Ru-cat at 900 nm in acetonitrile (A) and on ZrO_2 nanoparticle surface (B), after excitation at 400 nm.

SCHEME 1: Mechanistic Scheme Showing Three-Level Model Which Consists of the Ground State (S_0) State, the Excited Triplet State ($^3\text{MLCT}$) State, and the Excited Singlet ($^1\text{MLCT}$) State of Ru(II)–Polypyridyl Catecholate Adsorbed on TiO_2 Nanoparticles^a



^a The photon excites the electron from the S_0 state to the $^1\text{MLCT}$ state. Intersystem crossing (ISC) from nonthermalized $^1\text{MLCT}$ state to nonthermalized $^3\text{MLCT}$ state is very fast. Electron injection process competes with thermalization process of the excited states due to strong coupling of the dye–nanoparticle system. Single-exponential electron injection takes place from both nonthermalized $^1\text{MLCT}$ state and nonthermalized $^3\text{MLCT}$ state. No electron injection was observed from thermalized excited states.

attributed to the formation of singlet and/or triplet state. However, the second component grows with time constant of ~ 19 ps in acetonitrile and ~ 10 ps on the ZrO_2 nanoparticle surface. We have observed in Scheme 1 that the energy level of excited triplet state ($^3\text{MLCT}$) is around -0.68 V. As a result, upon excitation of Ru-cat at 400 nm, vibrationally hot (non-thermalized state) molecules of Ru-cat are created. This non-thermalized molecule will take some time to relax down to the thermalized state. This is typically known as vibration relaxation. Hence, the second growth constant in Figure 3A,B can be ascribed to vibration relaxation or can be due to relaxation within the triplet manifolds of the $^3\text{MLCT}$ state. It is interesting to observe that the relaxation is faster on nanoparticle surface (ZrO_2) as compared to that in solution. It is seen from Figure 3 that both the kinetic traces do not decay until 460 ps. It is

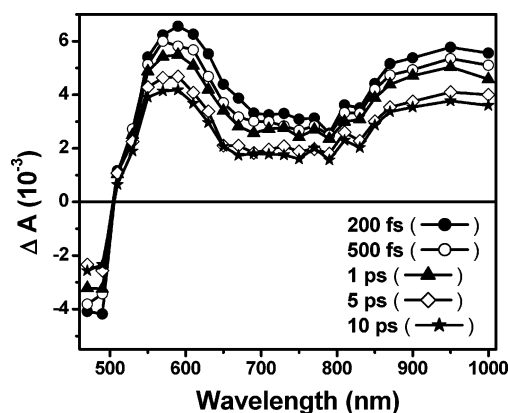


Figure 4. Transient absorption spectra of Ru-cat-sensitized TiO_2 nanoparticle in water at different time delays after excitation at 400 nm. The spectrum at each time delay consists of a bleach at 470–500 nm region centered at 480 nm, an absorption peak at 590 nm, and a broad positive absorption feature in the whole spectral region (700–1000 nm). These features are assigned to the ground-state bleach of Ru-cat dye, cation radical of Ru-cat, and injected electron in nanoparticles, respectively. A typical concentration of the TPP-cat molecules was $\sim 200 \mu\text{M}$ and TiO_2 particles was $\sim 20 \text{ g/L}$.

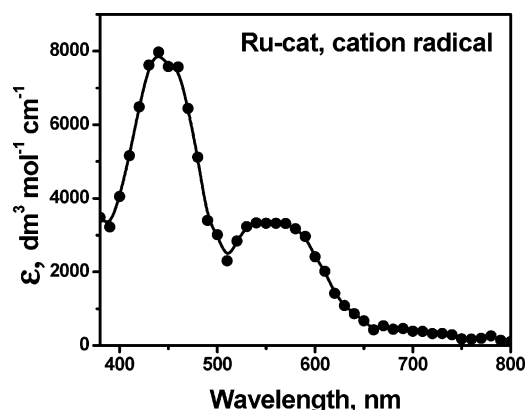


Figure 5. Transient absorption spectrum of the cation radical of Ru-cat obtained from one-electron oxidation in pulse radiolysis.

reported in the literature³⁶ that the lifetime of the triplet state ($^3\text{MLCT}$) of the Ru–polypyridyl complexes are $>100 \text{ ns}$ or so. The longer lifetime of the triplet state has been reflected, as the kinetic traces in Figure 3 do not decay up to 460 ps.

(c) Transient Absorption Measurements of Ru-cat/ TiO_2 . We have carried out transient absorption experiments for Ru-cat-sensitized TiO_2 nanoparticles exciting at 400 nm to follow the interfacial ET dynamics on a semiconductor surface. Figure 4 shows the transient absorption spectra of Ru-cat-sensitized TiO_2 nanoparticles at different time delay. The spectrum at each time delay consists of bleach in the 470–500 nm wavelength region with a maximum at ca. 480 nm, an absorption peak at ca. 590 nm, and another broad positive absorption band in the 700–1000 nm region. The absorption peak at 590 nm has been assigned to Ru-cat cation radical. Assignment of this band has been made on the basis of the results obtained in a complementary pulse radiolysis experiment, where Ru-cat $^{\bullet+}$ was generated selectively by the reaction of N_3 radical with Ru-cat molecule in N_2O -saturated aqueous solution (5% acetonitrile + 95% water). Figure 5 shows the corrected transient absorption spectrum for the Ru-cat $^{\bullet+}$ with absorption peak at 440 and 570 nm as obtained from pulse-radiolysis experiments. The extinction coefficient of cation radical has been found to be $\sim 3600 \text{ dm}^3 \text{ mol}^{-1} \text{ cm}^{-1}$ at 570 nm (Figure 5). However, on nanoparticle surface transient spectra can be broad and red-shifted as has

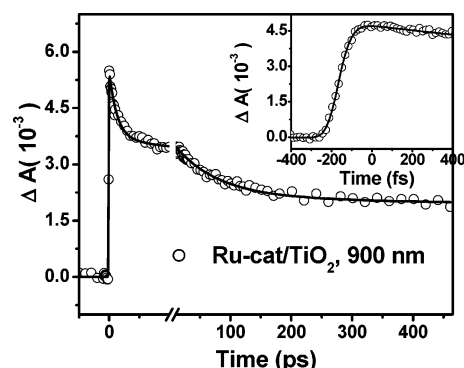


Figure 6. Kinetic decay trace of the injected electron in the conduction band at 900 nm in Ru-cat-sensitized TiO_2 nanoparticles exciting with 400 nm laser pulse. Inset shows the kinetic trace at 900 nm at shorter time scale.

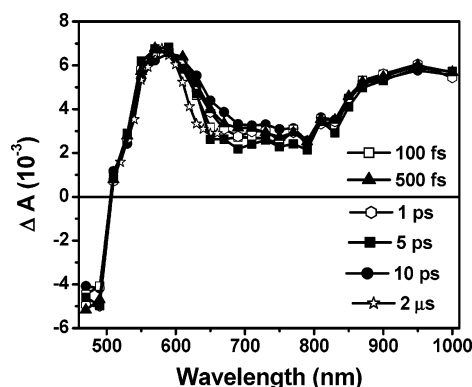


Figure 7. Normalized transient absorption spectra at various time delays of Ru-cat-sensitized TiO_2 nanoparticles (time scales: 100 fs, 500 fs, 1 ps, 5 ps, 10 ps, and 2 μs). The microsecond spectrum has been obtained after exciting the Ru-cat/ TiO_2 system at 532 nm.

been observed in Figure 4. The broad absorption band in the 700–1000 nm region has been attributed to the conduction band electrons in the nanoparticles.^{22,37,38} It has already been shown by us and many other groups that conduction band electrons can be detected by visible,^{22,37,38} near-IR,⁸ and mid-IR^{9,10} absorption. The injection time in the present investigation has been determined by monitoring the appearance time of the signal of the injected electron. The inset of Figure 6 shows the kinetic trace of the injected electron at 900 nm. The injection time has been found to be pulse width limited ($<100 \text{ fs}$) and single exponential. We have also monitored the appearance signal of the cation radical at 570 nm, and it is also found to be single exponential and pulse width limited similar to the electron signal at 900 nm.

At this juncture, it is important to clarify that the transient absorption observed in Figure 4 is primarily due to charge-separated species (cation radical and injected electron), and the contribution due to excited states is negligible. For the sake of the visualization of the processes, the transient absorption spectra at different delay given in Figure 4 are shown in the normalized mode in Figure 7. It is clear from the figure that the observed transients at different time delay (100 fs to 10 ps) are basically the same. Further, we have carried out transient absorption measurements in longer time domain ($>500 \text{ ns}$) in an effort to reveal that the observed transient species are due to charge-separated species only. This is due to the fact that the excited states (singlet and triplet) of Ru-cat will not persist up to that time, as the lifetime of excited triplet state is less than 500 ns. Time-resolved microsecond flash photolysis experiments have been carried out on Ru-cat-sensitized TiO_2 nanoparticle after

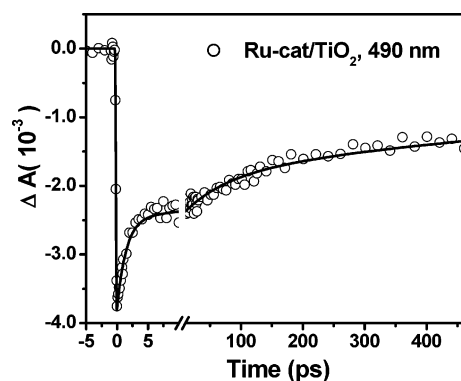
TABLE 1: Lifetimes of the Transients of Ru-cat-Sensitized TiO₂ Nanoparticles after Exciting with 400 nm (fwhm ~ 100 fs) Laser Pulse

wavelength, nm	lifetimes (ps)
900	$\tau_1 = 1.5$ (34.8%), $\tau_2 = 70$ (26.8%), $\tau_3 > 400$ (38.4%)
570	$\tau_1 = 1.5$ (36.5%), $\tau_2 = 70$ (25.6%), $\tau_3 > 400$ (37.9%)
490	$\tau_1 = 1.5$ (37.6%), $\tau_2 = 70$ (19.4%), $\tau_3 > 400$ (43%)

exciting with 532 nm laser pulse. Figure 7 shows the transient absorption spectra of the charge-separated species at 2 μ s. It is interesting to see the match between the transient absorption spectrum observed at 100 fs and 2 μ s. However, a close look at Figure 7 indicates that there is a change in the width of the cation spectrum in the 500–700 nm region from 100 fs to 2 μ s. From this observation one might think that there may be overlap of excited-state absorption with the cation radical in the early time domain. However, it is observed in Figure 7 that spectral difference occurs only in the red region (570–700 nm) of the cation radical spectra. If there were contribution from both excited singlet state and cation radical in early time spectra, then we would have seen difference in entire spectral region (470–1000 nm). However, we did not observe any difference in the 470–570 and 800–1000 nm spectral regions. The above observation can be explained as follows. As we are injecting electron in the TiO₂ nanoparticles from the unthermalized states of the dye molecules, it is quite possible that we can make the unthermalized cation radical of dye molecules, which will relax in due course of time to give a thermalized cation radical. This thermalization process is confirmed from the change in the red region of the cation radical spectrum. As a result, we have observed the narrowing of the cation radical absorption. However, it is interesting to observe that the normalized spectrum in the 800–1000 nm region in different time delays matched very well, which is absorption due to the injected electron only. Now at this juncture we would like to point out that if there were some contribution due to photoexcited Ru-cat in the Ru-cat/TiO₂ system, then the normalized spectrum at the 800–1000 nm region would not have matched at different time delay (Figure 7). These results unambiguously suggest to us that the transients observed at 100 fs are primarily due to charge-separated species.

It is reported by Sundstrom and co-workers that electron injection is multiphasic in N3-sensitized TiO₂ film, where electron injection takes place both from nonthermalized and thermalized excited states. Slower electron injection from thermalized triplet states has been confirmed by the decay of triplet states with a concomitant growth of cation radicals.¹³ However, in the present investigation, we did not observe any such concomitant growth for the cation radical or injected electron. Transient absorption at different wavelengths from 550 to 1000 nm decay with exactly similar time constants. It is seen in Table 1 that the decay kinetics at 570 and 900 nm exactly matches recovery kinetics at 490 nm. This observation clearly indicates that electron injection from thermalized triplet state is a remote possibility, and the majority of injection takes place from nonthermalized excited states.

The next important parameter in interfacial ET is the BET from the nanoparticles to the parent cation. Recombination dynamics (BET) can be determined by monitoring the decay kinetics of electron in the conduction band at 900 nm or cation radical at 570 nm or following the bleach recovery kinetics at 480 nm. To reconfirm the decay of the excited states at different wavelengths are only due to charge recombination (BET), it is important to know the molar extinction coefficients of excited species and also the cation radical of Ru-cat. We have already

**Figure 8.** Bleach recovery kinetics at 490 nm of Ru-cat-sensitized TiO₂ nanoparticle.

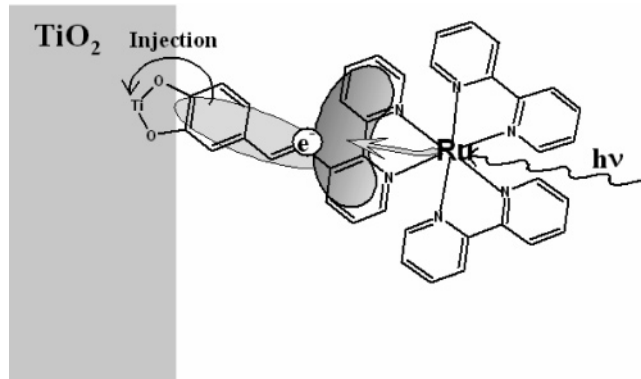
observed that the molar extinction coefficient of cation radical at 570 nm is $\sim 3600 \text{ dm}^3 \text{ mol}^{-1} \text{ cm}^{-1}$ as determined by the pulse-radiolysis technique. We have also determined the molar extinction coefficient of excited states of Ru-cat, and it is found to be $1900 \text{ dm}^3 \text{ mol}^{-1} \text{ cm}^{-1}$ at 590 nm using the perylene singlet state ($1.3 \times 10^4 \text{ dm}^3 \text{ mol}^{-1} \text{ cm}^{-1}$ at 710 nm) as standard in femtosecond transient absorption measurements. It is interesting to see that the molar extinction of the cation radical of Ru-cat is higher as compared to the excited states. So, if at all there is electron injection from the thermalized excited states, one would have seen the growth of the cation radical in early time scale (< 10 ps). However, we did not observe any such growth in transient absorption spectra. Hence, the decay of the transient species at different wavelengths is primarily due to charge recombination. Figure 6 shows the kinetic decay trace of conduction band electron at 900 nm. It has been observed that the kinetic decay trace follows a multiexponential function with the time constants of 1.5 ps (34.8%), 70 ps (26.8%), and > 400 ps (38.4%) (Table 1). Bleach recovery kinetics at 480 nm has been monitored, and it is shown in Figure 8. Here the recovery kinetics also have been fitted with a multiexponential time constants 1.5 ps (37.6%), 70 ps (19.4%), and > 400 ps (43%) (Table 1). We have also monitored the kinetic decay trace of the cation radical at 570 nm, and the fitted multiexponential time constants are reported in Table 1. It is very interesting to see that the bleach recovery kinetics and transient decay kinetics of injected electron and cation radical follow similar dynamics.

(d) Interfacial Charge Transfer. Charge-transfer dynamics in Ru-(dcbpy)₂(NCS)₂ (widely known as Ru-N3)-sensitized TiO₂ nanomaterials has been a subject of intense research interest for the past 10 years. Much of the recent work has focused on quantifying the rate of excited-state electron injection into the semiconductor^{8–13,39} and mechanistic details of charge recombination.^{11,40} In the above system, different electron injection rates have been reported. It has been shown by femtosecond transient near-IR spectroscopy that at least in some cases⁸ injection is ultrafast and occurs prior to vibrational relaxation to the thermally equilibrated MLCT manifold, i.e., from “hot” excited states or the Franck–Condon state itself. However, most of the authors agreed on the presence of the sub-100 fs component and considered it to be the dominant channel with additional contributions of slower nonexponential electron injection with a distribution of characteristic times from 1 ps to tens of picoseconds. The origin of the discrepancy of different electron injection dynamics is still under debate. In most of the studies it has been observed that injection dynamics is ultrafast and biphasic. Two assumptions have been made to explain the origin of the lack of single exponentiality: (i) because of the inhomogeneity of the semiconductor surface, the adsorbed dye

molecules have different geometric configurations resulting in different electronic coupling elements, giving rise to different rates, and (ii) the fast and slow components are due to electron injection from nonthermalized $^1\text{MLCT}$ and thermalized $^3\text{MLCT}$ states, respectively. However, most of the researchers believe in the second hypothesis, where competition between ET from the nonthermalized states and ISC to triplet states, vibrational cooling, or thermalization of triplet states is seen. Recently, Bhasikuttan et al.³⁵ have observed that ISC process of N3 dye can be as fast as <50 fs. So it can really compete with the electron injection process. It has been clearly demonstrated by Benko et al.¹³ that electron injection in the N3/TiO₂ system occurs mainly from the nonthermalized $^1\text{MLCT}$ state with a smaller contribution from the $^3\text{MLCT}$ state. Most of the researchers prefer to attribute biphasic injection by the second mechanism as suggested above, i.e., injection from $^1\text{MLCT}$ and $^3\text{MLCT}$ rather than the inhomogeneities of the semiconductor surface. In their studies¹³ they have also suggested that intramolecular processes such as ET reaction between the bipyridine ligands, i.e., interligand ET (ILET),^{41,42} control the triplet channel of electron injection. In a recent work, they have shown that the slower channel of injection is the result of the excited state being localized on a ligand of the sensitizer that is not attached to the semiconductor from where direct electron injection is not possible.⁴³ So the electron has to be transferred from the nonsurface-attached ligand to the attached one before injection. This ILET process plays a major role in the slow injection process in Ru–polypyridyl complex-sensitized TiO₂ nanocrystalline systems.

One of the central points of this investigation is whether it is possible to observe single-exponential electron injection from the photoexcited polypyridyl dyes to the conduction band of TiO₂ nanoparticles at all. The answer is affirmative, provided it has to fulfill certain conditions. Lian and co-workers have smartly demonstrated that if the $^3\text{MLCT}$ state of an adsorbate lies substantially below the conduction band edge, then one can suppress the slow component; as a result, the electron injection will be dominated by the fast component. They have observed this phenomenon in Re–carbonyl complexes (ReCO) on dry TiO₂ film,^{44–47} where ReCO's relaxed excited state is estimated to be -0.35 V (SCE) lower than that of TiO₂ dry film (-0.5 V at pH 2). However, in the present investigation, the relaxed $^3\text{MLCT}$ state of Ru-cat lies above the conduction band edge (Scheme 1). So, in principle it cannot fulfill the condition, which has been demonstrated by Lian and co-workers in ReCO complexes on TiO₂ film. On the other hand, in our earlier studies, we have observed single-exponential electron injection time constant in many organic dye–nanoparticle systems,^{18,19} where electron injection would only take place from the singlet excited state since the singlet–triplet ISC takes a long time (>1 ns). In those systems strong electronic coupling of the dye molecules with the nanoparticles would govern the electron injection dynamics. Strong coupling facilitates ultrafast electron injection from excited singlet state before it relaxes to the relaxed state. In the present investigation, we have observed that injection dynamics is single exponential and pulse-width limited (inset of Figure 6). Even though the Ru-cat complex can have both singlet ($^1\text{MLCT}$) and triplet ($^3\text{MLCT}$) manifold in the excited states, we still have observed a single component in the injection kinetics. Optical absorption studies have confirmed that Ru-cat binds strongly with the nanoparticles though the pendant catechol moiety. We have discussed earlier that catecholate binding ensures strong coupling for ET reaction. Although, it is reported earlier¹³ in the Ru–polypyridyl–TiO₂

SCHEME 2 : Mechanistic Scheme Showing the Various Processes Involved in the Electron Transfer Dynamics of Ru-cat to TiO₂ Nanoparticles Exciting at 400 nm^a



^a Following MLCT excitation of the Ru-cat-sensitized TiO₂ particles, an electron is promoted to the π^* state of the bp-cat ligands. Afterward, electron injection takes place from bpy-cat ligand (bind with TiO₂ through catechol moiety). Redox potential of bpy-cat (-1.09 V) is lower than the other two coordinated bpps (-1.193 and -1.59 V), so upon excitation electron in the excited state will be preferably localized very fast to the bpy-cat ligand. As a result, the entire electron injection process can take place (from nonthermalized $^1\text{MLCT}$ state) through catechol moiety due to strong coupling.

system electron injection from $^1\text{MLCT}$ (singlet) state competes with the ISC process to the $^3\text{MLCT}$ (triplet) state. In the present investigation due to the very fast ISC process, nonthermalized excited states can be due to both nonthermalized $^1\text{MLCT}$ (singlet) and nonthermalized $^3\text{MLCT}$ (triplet) states or a combination of both hot singlet and triplet states (Scheme 1). As a consequence of large electronic coupling in the present Ru-cat/TiO₂ system, electron injection is taking place predominantly from nonthermalized states (Scheme 1) rather than from thermalized states. It is reported in the literature¹⁶ that on excitation of the MLCT band of Ru–polypyridyl complexes the electron gets excited from the Ru metal center and localized in the bipyridyl ligands. So it is quite obvious that on excitation with 400 nm laser light the electron from the Ru(II) gets localized in one of the bipyridyl (bpy) ligands and also in the bpy-cat ligand. As bpy-cat is directly and strongly coupled with the TiO₂ nanoparticles, the injection process will take place from the bpy-cat ligand (TiO₂ surface attached ligand). On the other hand, the other two bpps are not attached directly with the nanoparticle so the deexcitation process from singlet to triplet manifold is possible. However, the redox potential of bpy-cat ligand is lower (-1.09 V) as compared to those of other bpy ligands (-1.19 and -1.59 V);⁴⁸ as a result, upon excitation, the photoexcited electron from ruthenium metal ion will prefer to get localized mostly at the bpy-cat ligand, from where fast electron injection will take place due to direct coupling with the nanoparticles (Scheme 2). As the localization takes place mostly on the bpy-cat ligand, the ILET process will not interfere much in the electron injection process at least for the present system. As a consequence, we have observed single-exponential and pulse width limited electron injection kinetics.

Now, let us discuss the charge recombination (BET) dynamics in the Ru-cat–TiO₂ system. The BET reaction between injected electrons and oxidized dye molecules is thought to be one of the main pathways of loss mechanisms in dye-sensitized solar cells. The dynamics of BET process has been determined by monitoring either the decay of conduction band electron or the oxidized state of dye or the bleach recovery of the ground state. We have monitored all the transients in different wavelengths, and the respective time constants are provided in Table 1.

Interestingly, in all the wavelengths, the transients' decay/recovery kinetics matched pretty well, which indicate that excited-state dynamics of Ru-cat/TiO₂ is related only to the ET process. It has been observed from Table 1 that recombination dynamics at 900 nm has been best fitted with multiexponential function with time constants of 1.5 ps (34.8%), 70 ps (26.8%), and >400 ps (38.4%). It is very interesting to observe that recombination dynamics in the Ru-cat/TiO₂ system is faster as compared to other Ru–polypyridyl complex (like N3)-sensitized TiO₂ nanoparticles systems.⁹ Although most of the N3 and other related complex/TiO₂ systems have been carried out on film, where recombination reaction is rather slow. In general, BET dynamics is faster in nanoparticles as compared to the film because the diffusion of injected electron is more in the film than in nanoparticles. Still we have observed that charge recombination is higher in the present investigation. In the carboxylate anchored Ru–polypyridyl complex-sensitized TiO₂ system, coupling strength for ET reaction is much lower as compared to that in catechol group anchored complex. As we have observed, strong binding of the catechol group with nanoparticles helps ultrafast single-exponential injection. Similarly, it has been observed that stronger binding of the catechol group also influences the BET dynamics, making it to be faster.

(e) Energy Conversion Implications. The significant application of the knowledge of interfacial ET reaction of dye-sensitized nanoparticle is to design and optimize the dye-sensitized solar cell. Most of the solar cells designed out of Ru–polypyridyl complex-sensitized TiO₂ crystalline film are carboxylate. However, the carboxylate sensitizers have low pK_a (3.5⁴⁹) values, so it can be easily desorb out of the TiO₂ film at higher pH conditions (>4). This may be the main drawback of the carboxylate dyes to use as a solar dye. On the other hand, the design of a solar dye with catechol as anchoring group can be of great help, where desorption of the dye molecules from the film surface will not take place until pH 9.6. So it can be a good candidate to design model sensitizers with high incident photon-to-current conversion efficiency. Ru(II)–polypyridyl complexes with a pendant catechol moiety can show considerable promise in the development of photovoltaic cells. Recently, Rice et al.⁷ designed a solar cell where Ru–polypyridyl complexes were anchored with the TiO₂ nanoparticles through a pendant catechol moiety. Despite very effective anchoring of the complexes onto surface, the measured IPCE values are lower than those obtained in related complexes with carboxylate anchor groups. From their investigation⁷ the real reason for lower efficiency was not clear. Our present investigation on ultrafast transient absorption experiments of the Ru-cat/TiO₂ system have showed that charge recombination reaction is relatively faster as compared to other Ru–polypyridyl complexes (like N3) with a carboxylate anchoring group. It can be inferred that fast BET may be the main reason for low efficiency. Because of the higher affinity and electronic coupling of the dye with TiO₂, the reaction falls in the adiabatic region of interfacial ET which leads to a faster BET rate. The faster BET rates eventually diminish the photovoltage yield and therefore decrease the energy conversion efficiency. Large electronic coupling indeed increases the forward ET rate but also increases the BET rate. Introduction of spacer in the bridging ligand can reduce the electronic coupling, which could decrease the BET rate and eventually can increase the energy conversion efficiency. It has been observed by Asbury et al.⁵⁰ that introducing the spacer in the bridging ligand diminishes the forward ET rates (electron injection). We are on the way of

making new derivatives of catechol–Ru–polypyridyl complexes by introducing spacer groups, which will help to retard BET reaction in the dye–nanoparticles system, which in turn will increase the efficiency for energy conversion.

4. Conclusion

The Ru(II)–polypyridyl complexes [$\{bis(2,2'-bpy)-(4-[2-(4'-methyl-2,2'-bipyridinyl-4-yl)vinyl]benzene-1,2-diol)\}$ ruthenium-(II) hexafluorophosphate] (Ru-cat) couple strongly with TiO₂ nanoparticles as the dye absorbed on the nanoparticle surface through pendant catechol moiety. As the pK_a value for the catechol ruthenium polypyridyl complex is as high as >9.5, this particular dye–nanoparticle system gives more stability even at higher pH conditions unlike other carboxylate–ruthenium–polypyridyl complexes. Femtosecond transient absorption measurements have been carried out to study interfacial ET dynamics in the Ru-cat/TiO₂ system. On excitation with the 400 nm laser pulse, a bleach of the adsorbed dye, transient absorption for the dye cation, and broad absorption band for the conduction band electron have been observed for the above dye–nanoparticle system. Electron injection is found to be single exponential and pulse width limited (<100 fs). In the present investigation electron injection process competes with the thermalization process in the photoexcited state of Ru-cat. Our results indicate that electron injection take place predominantly from the nonthermalized singlet state (¹MLCT) and/or the nonthermalized triplet state (³MLCT) or a combination of both, which is a unique observation in ET dynamics in Ru–polypyridyl/TiO₂ systems studied so far. Strong coupling in the dye–nanoparticle system facilitates ultrafast single-exponential electron injection, which competes with thermalization process of the excited states. We have determined BET dynamics by monitoring the decay kinetics of cation radical and/or injected electron and also from the recovery kinetics of the bleach of the adsorbed dye which found to be a multiexponential process with time constants of 1.5 ps (34.8%), 70 ps (26.8%), and >400 ps (38.4%). Strong coupling for the dye–nanoparticle system is responsible for fast charge recombination reaction.

Acknowledgment. We thank one of the reviewers for his constructive suggestions on the work, which have significantly improved the quality of the paper. We thank Dr. T. Mukherjee, Director, Chemistry Group, Bhabha Atomic Research Center, for his constant encouragement. A.D. thanks DST and BRNS while H.N.G. thanks BRNS for financial assistance.

Note Added after ASAP Publication. This article was released ASAP on July 21, 2005. The author name K. Krishna Kumar has been changed to D. Krishna Kumar and the Centre for Salt and Marine Chemicals Research Institute in the address line has been changed to the Central Salt and Marine Chemicals Research Institute. The correct version was posted on August 3, 2005.

References and Notes

- (1) Pelizzetti, M.; Schiavello, M. *Photochemical Conversion and Storage of Solar Energy*; Kluwer: Dordrecht, 1997.
- (2) Kalyansundaram, K.; Grätzel, M. *Coord. Chem. Rev.* **1998**, 77, 347.
- (3) O'Regan, B.; Grätzel, M. *Nature (London)* **1991**, 353, 737.
- (4) Nazeeruddin, M. K.; Pechy, P.; Renouard, T.; Zakeeruddin, S. M.; Humphry-Baker, R.; Comte, P.; Liska, P.; Cevey, L.; Costa, E.; Shklover, V.; Spiccia, L.; Deacon, G. B.; Bignozzi, C. A.; Grätzel, M. *J. Am. Chem. Soc.* **2001**, 123, 1613.
- (5) Nazeeruddin, M. K.; Humphry-Baker, R.; Grätzel, M.; Murrer, B. A. *Chem. Commun.* **1998**, 719.

- (6) Nazeeruddin, M. K.; Zakeeruddin, S. M.; Humphry-Baker, R.; Jirousek, M.; Liska, P.; Vlachopoulos, N.; Skhlover, V.; Fischer, C. H.; Gratzel, M. *Inorg. Chem.* **1999**, *38*, 6298.
- (7) Rice, C. R.; Ward, M. D.; Nazeeruddin, M. K.; Gratzel, M. *New J. Chem.* **2000**, *24*, 651.
- (8) Hannapel, T.; Burfeindt, B.; Storck, W.; Willig, F. *J. Phys. Chem. B* **1997**, *101*, 6799.
- (9) Asbury, J. B.; Hao, E.; Wang, Y. Q.; Ghosh, H. N.; Lian, T. *J. Phys. Chem. B* **2001**, *105*, 4545.
- (10) Asbury, J. B.; Ellingson, R. J.; Ghosh, H. N.; Ferrere, S.; Nozik, A.; Lian, T. *J. Phys. Chem. B* **1999**, *103*, 3110.
- (11) Tachibana, Y.; Moser, J. E.; Gratzel, M.; Klug, D. R.; Durrant, J. R. *J. Phys. Chem.* **1996**, *100*, 20056.
- (12) Kallioinen, J.; Lehtovuori, V.; Myllyperkio, P.; Korppi-Tommola, J. *Chem. Phys. Lett.* **2001**, *340*, 217.
- (13) Benko, G.; Kallioinen, J.; Korppi-Tommola, J. E. I.; Yartsev, A. P.; Sundstrom, V. *J. Am. Chem. Soc.* **2002**, *124*, 489.
- (14) Lu, H. P.; Xie, X. S. *J. Phys. Chem. B* **1997**, *101*, 2753.
- (15) Yeh, A. T.; Shank, C. V.; McCusker, J. K. *Science* **2000**, *289*, 935.
- (16) Rego, L. G. C.; Batista, V. S. *J. Am. Chem. Soc.* **2003**, *125*, 7989.
- (17) Wang, Y.; Hang, K.; Anderson, N. A.; Lian, T. *J. Phys. Chem. B* **2003**, *107*, 9434.
- (18) Ramakrishna, G.; Ghosh, H. N.; Singh, A. K.; Palit, D. K.; Mittal, J. P. *J. Phys. Chem. B* **2001**, *105*, 12786.
- (19) Ramakrishna, G.; Singh, A. K.; Palit, D. K.; Ghosh, H. N. *J. Phys. Chem. B* **2004**, *108*, 1701.
- (20) Shukla, A. D.; Whittl, B.; Bajaj, H. C.; Das, A.; Ward, M. D. *Inorg. Chim. Acta* **1999**, *285*, 89.
- (21) Bahnmann, D.; Henglein, A.; Lilie, J.; Spanhel, L. *J. Phys. Chem.* **1984**, *88*, 709.
- (22) Ghosh, H. N. *J. Phys. Chem. B* **1999**, *103*, 10382.
- (23) Ramakrishna, G.; Ghosh, H. N. *Langmuir* **2003**, *19*, 505.
- (24) Ramakrishna, G.; Singh, A. K.; Palit, D. K.; Ghosh, H. N. *J. Phys. Chem. B* **2004**, *108*, 4775.
- (25) Ramakrishna, G.; Singh, A. K.; Palit, D. K.; Ghosh, H. N. *J. Phys. Chem. B* **2004**, *108*, 12489.
- (26) Ghosh, H. N.; Pal, H.; Sapre, A. V.; Mittal, J. P. *J. Am. Chem. Soc.* **1993**, *115*, 11722.
- (27) Mukherjee, T. In Ahmad, S. A., Ed.; *Atomic, Molecular and Cluster Physics*; Narosa: New Delhi, 1997; p 299.
- (28) Hagfeldt, A.; Gratzel, M. *Chem. Rev.* **1995**, *95*, 49.
- (29) Bae, E.; Choi, W.; Park, J.; Shin, H. S.; Kim, S. B.; Lee, J. S. *J. Phys. Chem. B* **2004**, *108*, ASAP.
- (30) Will, G.; Boschloo, G.; Hoyle, R.; Rao, S. N.; Fitzmaurice, D. *J. Phys. Chem. B* **1997**, *102*, 10278.
- (31) Kleverlaan, C. J.; Indelli, M. T.; Bignozzi, C. A.; Pavanin, L.; Scandola, F.; Hasselman, G. M.; Meyer, G. J. *J. Am. Chem. Soc.* **2000**, *122*, 2840.
- (32) Cherepy, N. J.; Smestad, G. P.; Gratzel, M.; Zhang, J. Z. *J. Phys. Chem. B* **1997**, *101*, 9342.
- (33) Moser, J.; Punchedewa, S.; Infelta, P. P.; Gratzel, M. *Langmuir* **1991**, *7*, 3012.
- (34) Rajh, T.; Chen, L. X.; Lukas, K.; Liu, T.; Thurnauer, M. C.; Teide, D. M. *J. Phys. Chem. B* **2002**, *106*, 10543.
- (35) Bhasikuttan, A. C.; Suzuki, M.; Nakashima, S.; Okada, T. *J. Am. Chem. Soc.* **2002**, *124*, 8398.
- (36) Vlček, A., Jr. *Coord. Chem. Rev.* **2000**, *200*, 933.
- (37) Zhang, J. Z. *Acc. Chem. Res.* **1997**, *30*, 423.
- (38) Colombo, D. P., Jr.; Bowman, R. M. *J. Phys. Chem.* **1996**, *100*, 18445.
- (39) Kallioinen, J.; Benko, G.; Myllyperkio, P.; Khriachtchev, L.; Skarman, B.; Wallenberg, R.; Tuomikoski, M.; Korppi-Tommola, J.; Sundstrom, V.; Yartsev, A. P. *J. Phys. Chem. B* **2004**, *108*, in press.
- (40) Haque, S. A.; Tachibana, Y.; Willis, R. L.; Moser, J. E.; Gratzel, M.; Klug, D. R.; Durrant, J. R. *J. Phys. Chem. B* **2000**, *104*, 538.
- (41) Waterland, M. R.; Kelley, D. F. *J. Phys. Chem. B* **2001**, *105*, 4019.
- (42) Olsen, C. M.; Waterland, M. R.; Kelley, D. F. *J. Phys. Chem. B* **2002**, *106*, 1483.
- (43) Benko, G.; Kallioinen, J.; Myllyperkio, P.; Trif, F.; Korppi-Tommola, J.; Yartsev, A. P.; Sundstrom, V. *J. Phys. Chem. B* **2004**, *108*, 2862.
- (44) Asbury, J. B.; Hao, Y.; Wang, Y.; Lian, T. *J. Phys. Chem. B* **2000**, *104*, 11957.
- (45) Asbury, J. B.; Wang, Y.; Hao, E. C.; Ghosh, H. N.; Y.; Lian, T. *Res. Chem. Intermed.* **2001**, *27*, 315.
- (46) Asbury, J. B.; Anderson, N.; Hao, E. C.; Lian, T. *J. Phys. Chem. B* **2003**, *107*, 7376.
- (47) Anderson, N.; Lian, T. *Coord. Chem. Rev.* **2004**, *248*, 1231.
- (48) Lee, H. Y.; Kim, Y.; Dutta, P. K.; Das, A. *Inorg. Chem.* **2003**, *42*, 4215.
- (49) Montalti, M.; Wadhwa, S.; Kim, W. Y.; Kipp, R. A.; Schmehl, R. H. *Inorg. Chem.* **2000**, *39*, 76.
- (50) Asbury, J. B.; Hao, E.; Wang, Y.; Lian, T. *J. Phys. Chem. B* **2000**, *104*, 11957.